On the Role of Scattering Resonances in the F + HD Reaction Dynamics†

D. De Fazio,‡,§ S. Cavalli,‡ V. Aquilanti,‡ A. A. Buchachenko,|| and T. V. Tscherbul*,⊥

Dipartimento di Chimica, Università di Perugia, 06123 Perugia, Italy, Istituto di Metodologie Inorganiche e dei Plasmi - C.N.R., 70126 Bari, Italy, Laboratory of Molecular Structure and Quantum Mechanics, Department of Chemistry, Moscow State University, 119992 Moscow, Russia, and Department of Chemistry, University of British Columbia, V6T 1Z1, Vancouver, Canada

Received: July 27, 2007; In Final Form: October 2, 2007

We study scattering resonances in the F + HD → HF + D reaction using a new method for direct evaluation of the lifetime **Q**-matrix [Aquilanti et al., *J. Chem. Phys.* **2005**, *123*, 054314]. We show that most of the resonances are due to van der Waals states in the entrance and exit reaction channels. The metastable states observed in the product reaction channel are assigned by calculating the energy levels and wave functions of the HF···D van der Waals complex. The behavior of resonance energies, widths, and decay branching ratios as functions of total angular momentum is analyzed. The effect of isotopic substitution on resonance energies and lifetimes is elucidated by comparison with previous results for the F + H_2 reaction. It is demonstrated that HF($v' = 3$) products near threshold are formed by decay of the narrow resonances supported by van der Waals wells in the exit channel. State-to-state differential cross sections in the HF($v' = 3$) channel exhibit characteristic forward−backward peaks due to the formation of a long-lived metastable complex. The role of the exit-channel resonances in the interpretation of molecular beam experiments is discussed.

I. Introduction

The F + HD reaction has played a fundamental role in chemical physics since the 1985 molecular beam experiment of Lee and co-workers[1] in which vibrationally resolved integral cross sections (ICS) and angular distributions were measured for the first time. The experiment revealed an anomalous HF($v' = 3$) forward scattering peak which was interpreted to be a signature of a quantum-mechanical resonance. Later experiments demonstrated the effects of resonances on state-resolved differential cross sections (DCS),[2] total ICS,[2,3] and product vibrational distributions[4] as well as in the photodetachment spectrum of the F···H_2^- anion.[5] Extensive quantum mechanical simulations[2,3,6] on the potential energy surface of Stark and Werner (SW PES)[7] confirmed the existence of a transition state resonance[8] (peak A) which governs the reaction to form the HF product at low collision energies.[9] The resonance effect survives partial-wave averaging and produces a step-like feature in the reaction excitation function at a collision energy of 0.5 kcal/mol. The calculations[2,3] reproduced the energy of the peak, but its height and shape were not reproduced quantitatively. Reactive scattering calculations with PESIII,[10] a potential energy surface developed in our laboratory on the basis of semiempirical modifications of the SW PES in the entrance channel,[11,12] provided an improved agreement with experimental results. The larger barrier width of PESIII reduces the tunneling effect which leads to a decrease of the calculated ICS. However, the excellent agreement obtained with PESIII at collision energies below 1 kcal/mol does not extend to higher energies. In particular, the HF($v' = 3$) yield is significantly underestimated in theoretical calculations with all available PESs tested so far.[10] The inclusion of nonadiabatic couplings due to the spin−orbit and the open-shell structure of the fluorine atom did not resolve this discrepancy[13,14] which was attributed to inaccuracies in the description of the exit reaction channel.[15,16]

More recently, the F + HD reaction has been the subject of several experimental studies.[17−21] In a high-resolution crossed-beam study, Liu and co-workers[17] observed rotationally resolved DCS for the production of vibrationally selected HF($v' = 2$) at six collision energies below 1.2 kcal/mol. This work was later extended to higher collision energies (up to 4.5 kcal/mol).[18] The same group explored the reactivity of F atoms in the excited spin−orbit state,[19] and the role of the spin−orbit excitation in the production of HF($v' = 3$) products. Forward−backward peaks of the HF products were observed in the collision energy region between 1 and 2 kcal/mol,[18,19] which could result from a mechanism involving long-lived resonances. Narrow resonances are known to produce forward−backward structures in DCSs. For example, the insertion reactions O + H_2 → OH + H and N + H_2 → NH + H[22] display such behavior over a wide range of energies. Conversely, sharp forward−backward peaks in the DCSs may be a signature of the decay of metastable complexes.

At the energies of the experiment of Liu and co-workers,[18,19] a significant role in shaping the DCSs might be played by exit-channel van der Waals resonances.[23] These resonances have already been found in the F + HD reaction probabilities calculated on the SW PES for zero total angular momentum at collision energies higher than 1 kcal/mol.[24,25] The role of these resonances in the formation of the HF($v' = 3$) products was discussed by Castillo and Manolopoulos,[23] Dobbyn et al.,[26] and Sokolovsky.[27] However, their results were obtained at a single collision energy, and it was not clear whether the effects observed were important for the overall reactivity. Other quantum calculations[3,10,13,14] at several collision energies did not demonstrate significant resonance structure (except for the

† Part of the "Giacinto Scoles Festschrift".

* To whom correspondence should be addressed. E-mail: timur@chem.ubc.ca.

‡ Università di Perugia.

§ C.N.R.

|| Moscow State University.

⊥ University of British Columbia.

10.1021/jp0759473 CCC: $37.00
Published on Web 11/13/2007

transition state resonance mentioned above). Takayanagi has recently reported fully converged ICSs for the reaction of F with HD($v = 0$, $j = 0$) on a dense grid of collision energies and observed the resonance structure in the exit reaction channel.[28]

In this work, we perform a systematic analysis of scattering resonances in the F + HD reaction using a multichannel version of the time delay formalism proposed by Wigner.[29] Our approach involves the construction of the lifetime matrix **Q**[30] whose eigenvalues and eigenvectors are useful tools to characterize the resonance dynamics.[31−33] Recently, we have developed a direct and efficient method for numerical evaluation of the **Q**-matrix which allowed us to study resonances in the F + H_2 reaction.[33] Here, we extend this study to the F + HD ($v = 0, j = 0, 1$) reaction. We obtain energies, lifetimes and decay probabilities of reactive scattering resonances at collision energies below 100 meV.

The paper is organized as follows. In section II, we describe numerical details of our calculations and convergence tests, whereas section III presents the results. The effects of resonances on reactive scattering cross sections are discussed in section IV where we also compare the F + HD and F + H_2 reactions from the viewpoint of resonance dynamics.[33] The paper concludes (section V) with a short summary of the results and a discussion of the possible relevance of the studied metastable states in the interpretation of recent molecular beam experiments.[18]

II. Theory

For dynamical calculations, we use a potential energy surface (PESIII) based on the standard Stark-Werner potential,[7] semiempirically corrected in the entrance channel[34] to take into account the spin−orbit and long range interactions.[11,12] This PES provides a good agreement with experimental kinetic and molecular beam measurements for both F + HD[10] and F + H_2 reactions.[12,35] Also it is the same PES used in our previous calculation for the F + H_2 reaction[33] which will allow us in section IV A to examine in detail the effect of isotopic substitution on the resonance dynamics.

As pointed out in the introduction, some of the resonances studied in this paper were also observed in recent calculations using the SW PES.[28] The exit channel regions of the SW PES (and other PESs based on it[36,37]) and PESIII are almost the same, and the resonance patterns calculated with the two PESs are similar[38] (see ref 32 for a comparison of the F + H_2 resonances calculated on the two surfaces). Here, we perform a systematic assignment of the individual resonances and study their evolution with total angular momentum using the **Q**-matrix formalism and bound state calculations. Our studies thus complement the results of Takayanagi[28] and provide a wealth of additional information about narrow resonances in the F + HD reaction.

A. Dynamical Calculations and Convergence Tests. Quantum mechanical reactive scattering calculations are performed using symmetric hyperspherical coordinates and the hyperquantization algorithm.[39,40] In brief, the Hamiltonian of the three-body system at fixed hyperradius is diagonalized[41,42] and the resulting adiabatic functions are used as a basis to expand the total scattering wave function. The substitution of this expansion into the Schrödinger equation yields a system of close-coupled equations to be solved for each value of the total angular momentum J and the total inversion parity.

The hyperquantization parameters used in this work are listed in ref 10. However, to get convergent values of the resonance energies and lifetimes, the parameters that control the accuracy of the propagation step were modified. In particular, we used an evenly spaced grid of 400 points from 2.0 to 12.0 a_0 for the hyperradius (a factor of 8 larger that that of ref 10). The number of scattering channels was also increased, ranging from 400 for $J = 0$ to 2200 for $J \geq 3$. With this basis set, we obtain total ICSs and resonance parameters converged to within ~0.5%. The large basis set employed in the present work and the necessity to perform many scattering calculations to resolve narrow resonances made the calculations quite expensive. Therefore, we mainly focused on the metastable states which might be important for the interpretation of recent molecular beam studies of the F + HD reaction (see section IV.B).

B. Q-Matrix Analysis. The close-coupled equations were solved using the log-derivative method, which was extended to propagate the energy derivative of the hyperradial wave function.[33] This allowed us to generate both the scattering matrix S^J and its energy derivative $d\mathbf{S}^J/dE$ in a single calculation. To simplify the notation, we will omit the subscript J assuming that all calculations are performed at fixed J. The **Q**-matrix is evaluated from the **S**-matrix and its energy derivative[30]

$$\mathbf{Q} = -i\hbar\mathbf{S}^{\dagger}\frac{d\mathbf{S}}{dE_c} \tag{1}$$

and diagonalized as a function of the translational (collision) energy E_c to give the eigenlifetime spectrum. In the vicinity of an isolated narrow resonance, the largest eigenvalue of the **Q**-matrix q_{max} has a Lorentzian form

$$q_{max}(E_c) = \frac{\hbar\Gamma_r}{(E_c - E_r)^2 + \Gamma_r^2/4} + b(E_r) \tag{2}$$

where E_r is the resonance energy, Γ_r is its width, and $b(E_r)$ is a background contribution which is assumed to vary slowly compared to the first term. When two or more resonances overlap and/or interact,[43] the description in terms of several of the largest **Q**-matrix eigenvalues may be necessary.[32,44,45]

To study the resonance dynamics in the F + HD reaction, we diagonalized the **Q**-matrix on a dense grid of collision energies. The lifetime matrix formalism accounts for all resonances present in a triatomic system,[30] including those from the inelastic (nonreactive) blocks of the **S**-matrix. These metastable states will affect elastic and/or rovibrationally inelastic scattering in any of the three chemical arrangements. In order to affect the dynamics of a chemical reaction, a resonance state must decay into both the reactant and product channels. To identify such "reactive" resonances in the eigenlifetime spectrum, we use the **Q**-matrix eigenvectors[33]

$$\Lambda = \mathbf{T}^{\dagger}\mathbf{Q}\mathbf{T} \tag{3}$$

to define the branching probability for a resonance to decay into particular rovibrational channel (v, j) of arrangement α

$$P^Q(\alpha, v, j) = \sum_l |t_{\alpha vjl}|^2 \tag{4}$$

where l is the orbital angular momentum quantum number and t denotes the element of the matrix **T** from the column corresponding to the maximal eigenlifetime q_{max}.[33] If a resonance decays into one arrangement only, i.e., $P^Q(\alpha, v, j) \sim 1$ for some α, or it does not decay in the entrance channel, $P^Q(\alpha, v, j) \sim 0$ for $\alpha = 1$, it is considered as "inelastic" and excluded from our analysis.

III. Results

A. Reactive Resonances at $J = 0$. The largest eigenvalue of the **Q**-matrix as a function of collision energy E_c relative to

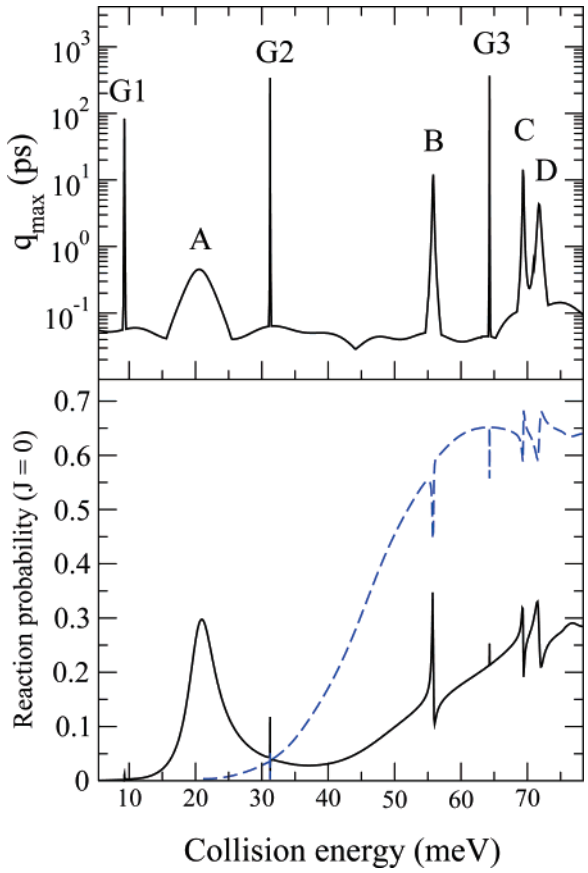

Figure 1. (Upper panel) The largest eigenvalue of the **Q**-matrix as a function of collision energy for the F + HD($v = 0$, $j = 0$) reaction at $J = 0$. Note the logarithmic scale used for the *y* axis. (Lower panel) Total $J = 0$ reaction probabilities for the formation of HF (solid line) and DF (dashed line).

the F + HD($v = 0$, $j = 0$) threshold is shown in the upper panel of Figure 1. Distinct peaks in the eigenlifetime spectrum correlate with those in the $J = 0$ reaction probabilities for the formation of both HF and DF products (lower panel). These structures are known as Fano profiles[46] and appear in the $J = 0$ reaction probabilities, as a result of interference between the background and resonance scattering. Otherwise, all lifetime peaks are perfectly Lorentzian. The energies and widths of the resonances obtained by fitting the peaks of Figure 1 (upper panel) to eq 2 are listed in Table 1.

The broad peak at $E_c \approx 21$ meV (denoted by A in the upper panel of Figure 1) was studied in great detail[2,3,6,8,9] on the SW PES. It was shown that the wave function of the resonance A is localized in the collinear configuration near the transition state closer to the product valley, with three nodes along the asymmetric stretching coordinate and no nodes along the bending coordinate. One particular aspect of this resonance is that it is practically unaffected by background scattering which results in a purely Lorentzian form of the reaction probability.[3] Moreover, it decays almost exclusively into the ground state of H_2 and into the $v' = 2$ vibrational state of HF thus affecting mainly the $v = 0$, $j = 0 \rightarrow v' = 2$ reactive transition.

Table 1 shows that the resonance A on PESIII is only slightly shifted with respect to the SW PES (21.5 meV[3,6]), whereas the resonance lifetime of 131.4 fs obtained for PESIII is significantly larger than the values 98[6] and 109[3] for the SW PES. The decay probabilities for PESIII are 0.9 (HF + D channel) and 0.1 (F + HD channel), versus 0.6 and 0.4 for the SW PES.[3,6] Because of the lower coupling with the reactants, the peaks in the reaction probabilities due to the resonance A are less pronounced for PESIII, in better agreement with experiment.[10] This effect can be easily related to the known differences between the two PESs. The spin−orbit interaction influences only the entrance channel of the reaction increasing the thickness of the reaction barrier. At the transition state, the spin−orbit interaction becomes negligible,[10,36] leaving the transition state properties unchanged. Therefore, although the energies of the resonance A are similar for the two PESs, the partial widths differ significantly because of the reduced tunneling effect that has a strong influence on the prereaction mechanism.[25]

The long-lived resonances denoted in Figure 1 as B, C, and D correspond to metastable states trapped in the exit-channel van der Waals well. As shown in the lower panel of Figure 1, the resonances show up in reaction probabilities for both product channels although the probability of the reaction to form H + DF is less affected. In the next subsection, we will explain this effect by analyzing the resonance wave functions. We note that the reaction probabilities of different product channels display inverted profiles because of the different background phases. The decay probabilities (7) summed over v and j are 0.55 (F + HD), 0.39 (HF + D), and 0.06 (DF + H) for the resonance B and 0.55 (F + HD), 0.35 (HF + D), and 0.09 (DF + H) for the resonances C and D. The decay of the resonances B, C, and D is less vibrationally specific than that of the resonance A: ~80% goes into the $v' = 2$ channel. When $v' = 3$ channel is energetically available (only for the resonance D at $J = 0$) a significant amount (around 15%) of the HF population resides in this channel.

The three narrow resonances ($\Gamma \sim 10^{-3}$ meV) at $E_c \sim 6$, 31, and 64 meV labeled as G1, G2, and G3 respectively, were studied for the first time by Takayanagi and Kurosaki.[24] The notation comes from our previous studies of the F + H_2 reaction[32,33] where similar peaks were observed and assigned. They are Feshbach resonances corresponding to metastable states in the van der Waals well of the entrance reaction channel and can be considered as a progression of "hindered rotor" states of HD ($v = 0$, j) with $j = 1$, 2, and 3, respectively. The F···HD($v = 0$, $j = 0$) van der Waals complex has a quasibound state close to the threshold which has a significant effect on chemical reactivity at low and ultralow temperatures.[47,48] The resonances G1 and G2 have a small (less than 5%) but significant decay probability into the HF product channel. Although the resonance G3 is more strongly coupled to the HF product channel [$\sum_{v,j} P^Q(\alpha = 2, v, j) = 0.11$], it mainly decays into higher rotational states of HD and as such it has the weakest effect on the reaction of F with HD($v = 0$, $j = 0$). Figure 1 and the corresponding data from ref 12 show that the entrance channel resonances are less pronounced for F + HD than for F + H_2 reaction. The weak coupling to the exit channel rapidly tends to zero with J, so that the effect of these resonances on the overall reactivity is expected to be small, and they will not be studied for $J > 0$ in this work.

B. Assignment of Resonances and Bound-State Calculations. *1. Adiabatic Model.* To assign quasimolecular quantum numbers to the resonance features B, C, and D shown in Figure 1, we use the same adiabatic model as in ref 32. In brief, the total Hamiltonian is constructed on a grid of R, the center-of-mass separation between the HF molecule, and the D atom. The matrix elements of the Hamiltonian are evaluated numerically in a space-fixed basis of rovibrational functions of HF($v' = 3$). The bound states are calculated by the Fourier grid method[49] which takes into account the couplings between different adiabatic states, unlike the model used in ref 50.

TABLE 1: Energies, Widths (at $J = 0$), and Rotational Constants of Reactive Scattering Resonances[a]

resonance	energy	width	lifetime τ, fs	rotational constant
A	20.55 (14.05)	5.01 (11.64)	131.4 (58)	0.219 (0.367)
B	55.80 (24.33)	0.198 (1.94)	3324 (350)	0.115 (0.216)
C	69.37 (34.59)	0.145 (0.072)	4539 (9400)	0.0766 (0.123)
D	71.77 (39.89)	0.584 (1.5 × 10^{-3})	1127 (-)	0.0860 (0.094)
G1	9.29 (-)	3.08 × 10^{-2} (-)	2.14 × 10^{4} (-)	- (-)
G2	31.24 (42.59)	6.52 × 10^{3} (5.5 × 10^{-3})	1.01 × 10^{5} (1.2 × 10^{5})	- (0.055)
G3	64.30 (-)	4.15 × 10^{-3} (-)	1.59 × 10^{5} (-)	- (-)

[a] The values are given in meV relative to the energy of the ground rotational state of the reactants. The results of ref 33 for the F + H_2 reaction are given in parentheses for comparison. The calculations are performed on PESIII.

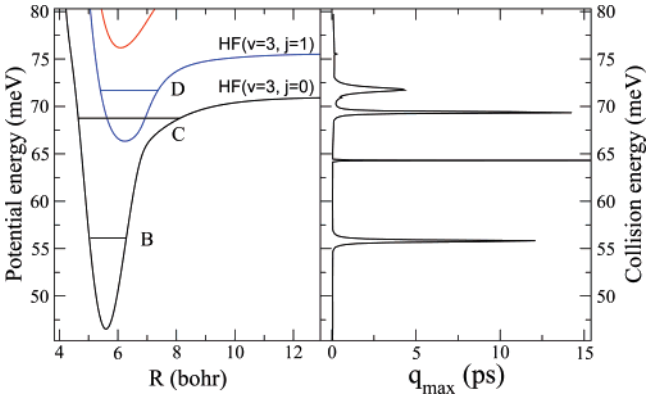

Figure 2. Lowest eigenvalues of the HF($v' = 3$)−D Hamiltonian as functions of the HF−D distance R (adiabatic curves). The bound levels shown in each curve are obtained by solving a set of coupled channel Schrödinger equations (see text). The bound levels B, C, and D correspond to the resonance peaks in the $J = 0$ eigenlifetime spectrum (right panel).

The lowest eigenvalues (adiabatic curves) of the Hamiltonian matrix for $J = 0$ are shown in Figure 2 as functions of R. The lowest-energy adiabatic curve has a depth of 24 meV and supports two bound levels corresponding to the peaks B and C in the right panel. This suggests that the peaks B and C are Feshbach resonances which can be assigned as (0,3,0) and (1,3,0) in the local mode picture. Here, the first quantum number refers to D−HF stretching vibration and the second and third numbers refer to DH−F stretching and HF bending (or hindered rotation about the D atom). The curve correlating to the HF($v = 3, j = 1$) threshold is shallower and supports only one bound state. We will call this resonance D following the F + H_2 terminology.[32,33] Applying the adiabatic model to the F···HD van der Waals complex in the entrance channel,[12] we can assign quasi-molecular quantum numbers to the narrow resonances $G1$, $G2$, and $G3$ as well.

2. Variational Calculations. In order to obtain the wave functions of the exit channel resonances B, C, and D, we performed two-dimensional (2D) variational calculations of the metastable states of the HF($v' = 3$)···D van der Waals complex. For this purpose, we used the Jacobi coordinates (r, R, θ) suitable for the HF + D arrangement, where r is the internuclear distance of HF, R is the distance between the D atom and the diatom center of mass, and θ is the angle between the corresponding Jacobi vectors. In the molecule-fixed frame with the z axis pointing along the **R** vector, the total Hamiltonian takes the form[51]

$$\hat{H} = -\frac{1}{2m_{\mathrm{HF-D}}}\frac{\partial^2}{\partial R^2} - \frac{1}{2m_{\mathrm{HF}}}\frac{\partial^2}{\partial r^2} + \frac{(\mathbf{J}-\mathbf{j})^2}{2m_{\mathrm{HF-D}}R^2} + \frac{\mathbf{j}^2}{2m_{\mathrm{HF}}r^2} + U(r) + V(r, R, \theta) \quad (5)$$

where m_{HF} and $m_{\mathrm{HF-D}}$ are the two-body reduced masses of the HF molecule and the triatomic system HF−D, respectively, **j** and **J** denote the rotational momenta of the diatomic fragment and of the whole complex, and the total three-dimensional potential is separated into the internal HF potential $U(r)$ and the atom-molecule interaction potential V. In order to investigate the resonances in the exit reaction channel, we used the diabatic approximation for the HF vibrational motion.[51] The Hamiltonian (5) is averaged over the vibrational function of the HF fragment χ_v, the eigenfunction of the total Hamiltonian in the asymptotic $R \rightarrow \infty$ limit, to yield

$$\hat{H} = -\frac{1}{2m_{\mathrm{HF-D}}}\frac{\partial^2}{\partial R^2} + \frac{(\mathbf{J}-\mathbf{j})^2}{2m_{\mathrm{HF-D}}R^2} + B_v\mathbf{j}^2 + U(r) + V_{vv}(R, \theta) \quad (6)$$

where $B_v = \langle\chi_v|m_{\mathrm{HF}}r^{-2}|\chi_v\rangle$ and $V_{vv} = \langle\chi_v|V(r, R, \theta)|\chi_v\rangle_r$. Again as in the adiabatic model, only the wave function for $v' = 3$ is used.

The eigenvalue problem for the 2D Hamiltonian (6) is solved variationally using the radial basis functions for the Morse potential enclosed in a box with a width L and the symmetry-adapted angular basis functions.[51] Following Reid et al.,[52] the resulting rovibrational energy levels of the complex are classified as J^{p_i}, where J is the total angular momentum value and p_i corresponds to the total inversion parity $p = (-1)^J p_i$. The calculations were performed for the positive parity levels 0^+, 1^-, and 2^+. To locate the metastable states lying above the HF($v = 3$) + D limit, stabilization graphs are constructed by repeating the calculations with varying box size L. The two lowest roots below the HF($v = 3, j = 0$) + D asymptotic limit represent the ground $n = 0$ and first excited $n = 1$ states of the complex. They are stable within the 2D approximation (although they may decay through vibrational predissociation into the HF($v' = 2, j'$) + D products). The next root corresponds to a metastable state and lies slightly above the dissociation limit. The stabilized values are reported in Table 2. The energy of the third state splits for nonzero J due to the rotational and Coriolis couplings that lift the triple degeneracy of molecular channels.[33,53] At $J = 1$ two levels appear in the block of negative p_i parity (denoted as D_1 and D_2 in Table 2), while the third component manifests itself in the positive p_i block.

Table 2 compares 2D energies with the predictions of the adiabatic model and the results of the **Q**-matrix calculations. In general, the agreement among the three sets of data is good, confirming the accuracy of the models used. The adiabatic model is formally equivalent to a 2D variational calculation. In practice, however, the results of the two models are slightly different due to the different methods used to locate the resonance states. Using the 2D results for $J = 1$ and 2 from Table 2, we can evaluate the rotational constants of the complexes: $B_r(B) = 0.122$, $B_r(C) = 0.083$, and $B_r(D) = 0.094$

TABLE 2: Energies of the Three Lowest Resonances B, C, and D (in Units of meV) Relative to the HF($v = 3, j = 0$) Threshold

resonance	J	adiabatic model	variational calculation (2D)	lifetime analysis
B	0	−14.87	−14.77	−15.18
	1	−14.62	−14.54	−15.04
	2	−14.12	−14.03	−14.43
C	0	−2.22	−2.26	−1.59
	1	−2.05	−2.09	−1.43
	2	−1.72	−1.77	−1.08
D_1	0	0.71	0.71	0.81
	1	0.90	0.89	0.99
	2	1.27	1.33	1.42
D_2	1	1.88	1.82	2.81
	2	2.27	2.26	3.25

meV. The value of B_r for the B resonance is in excellent agreement with the scattering calculations from Table 1. The agreement between the stabilization and scattering data for the resonances C and D is less satisfactory because of their proximity to continuum.

Variational calculations allow for the interpretation of reactive scattering resonances as metastable states of weakly bound complexes in the product channel of the reaction. Figure 3 is a 3D plot of the squared wave function for three lowest levels of the HF($v = 3$)···D complex from the 0^+ block in Cartesian coordinates $X = R \cos \theta$, $Y = R \sin \theta$, where $\theta = 0$ and $\theta = \pi$ correspond to the collinear D···FH and D···HF configurations, respectively. The wave function of the ground level (B) is strongly localized in the deeper D···HF well in the collinear configuration. The second level (C) corresponds to the stretching excitation, as follows from the node along X coordinate. The stretching excitation energy is above the bottom of the secondary potential well in the opposite D···FH collinear configuration leading to strong delocalization along the angular coordinate. The wave function of the C resonance shown in the central panel of Figure 3 corresponds to almost free rotation of the D atom around the HF fragment. The wave function of the third level D is similar to that of the second but reveals additional bending excitation (a node close to $X = 0$ plane). However, it is more localized in the ground D···HF potential well.

The analysis of the resonance wave functions allows us to explain the presence of resonance peaks in the $J = 0$ reaction probability for the DF + H channel (shown in the lower panel of Figure 1). The resonance complex localized in the D···HF configuration may undergo a hindered rotation into the D···FH geometry before breaking up to form the DF + H products. The detailed picture of this "internal rotation" process depends on the potential wells separating these two limiting geometries. Similar tunneling processes were recently observed in weakly bound anionic complexes Cl^-···HD and Br^-···HD.[54,55]

C. *J*-Dependence of Resonance Properties. The lifetime spectrum at $J = 0$ presented above provides detailed information about the resonance dynamics. However, a resonance can only be considered important for the chemical reaction if it contributes significantly to the reaction probabilities at large values of the total angular momentum. Otherwise, the resonance is likely to be washed out by the averaging over partial waves. Since modern crossed-beam experiments are carried out in the multiple partial wave regime, it is important to understand how resonances change with increasing total angular momentum. To this aim, we performed lifetime calculations for the partial waves in the $J = 0-20$ range, which gives resonance contributions to the reaction cross section at collision energies under 100 meV.

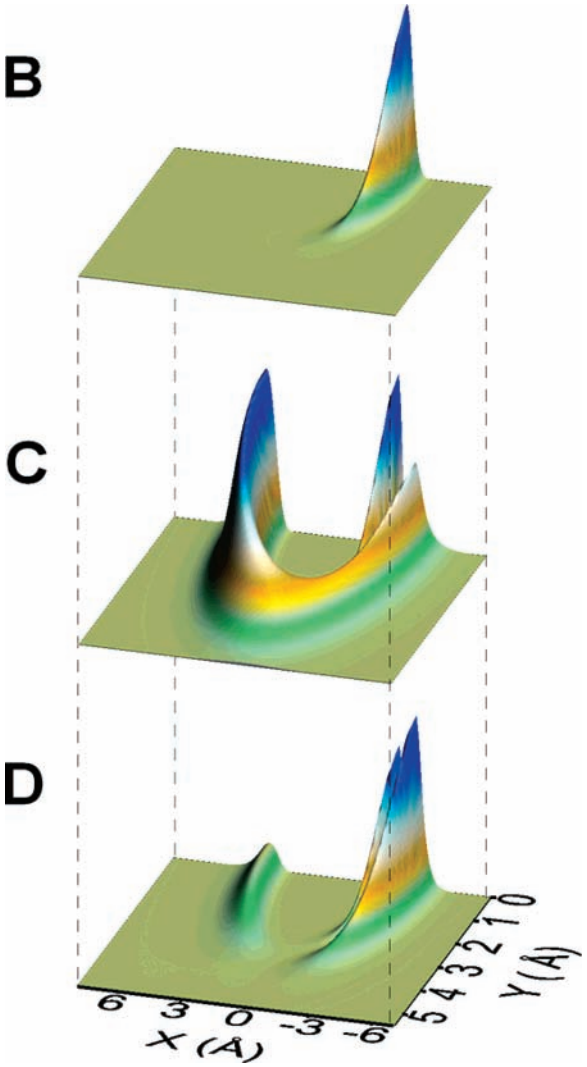

Figure 3. Squared wave functions of the metastable levels B ($n = 0$) (upper panel), C ($n = 1$) (middle panel), and D (lower panel) in the 0^+ parity block as function of $X = R \cos \theta$ and $Y = R \sin \theta$ (see text).

Figure 4 shows resonance energies as functions of $J(J + 1)$ for $J = 0-20$. All resonances follow closely the rigid-rotor behavior

$$E_r(J) = E_0 + B_r J(J + 1) \tag{7}$$

where B_r is the rotational constant, an important parameter characterizing the geometry of the resonance state. Linear fits to eq 7 are shown in Figure 4 as solid lines. The coefficients B_r are collected in Table 1. The resonance A has the largest rotational constant. This suggests that it may have an impact on reactive dynamics over a wide region of collision energies. On the other hand, the narrow resonances B, C, and D are likely to affect the reaction dynamics in a limited collision energy range.

The value of B_r is directly related to the geometry of the metastable complex

$$B_r = \frac{1}{2\mu_{FHD}\rho_0^2} \tag{8}$$

where μ_{FHD} is the hyperspherical three-body reduced mass of the FHD system, and $\rho_0^2 = \bar{\mathbf{R}}^2 + \bar{\mathbf{r}}^2$, where $\bar{\mathbf{R}}$ and $\bar{\mathbf{r}}$ are the values of mass-scaled Jacobi vectors at the equilibrium geometry of the complex. Using the parameters of the linear transition

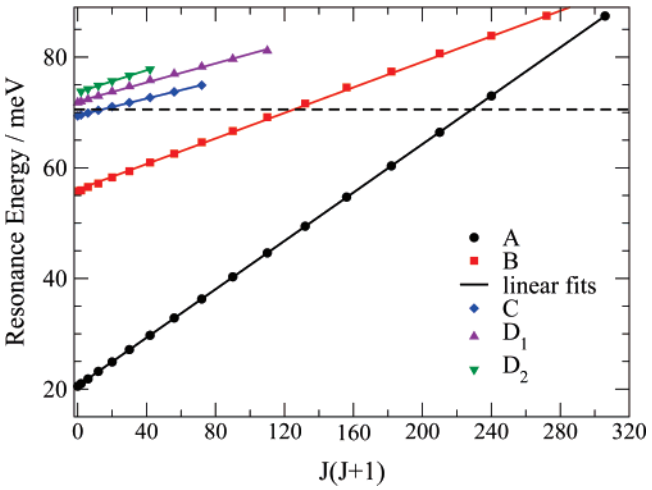

Figure 4. Resonance energies as functions of $J(J+1)$. Solid lines are the regression lines of the data required to get rotational constants given in Table 1. The dashed line marks the opening of the HF($v' = 3, j' = 0$) channel. Diffent symbols refer to different metastable states labeled on the graph.

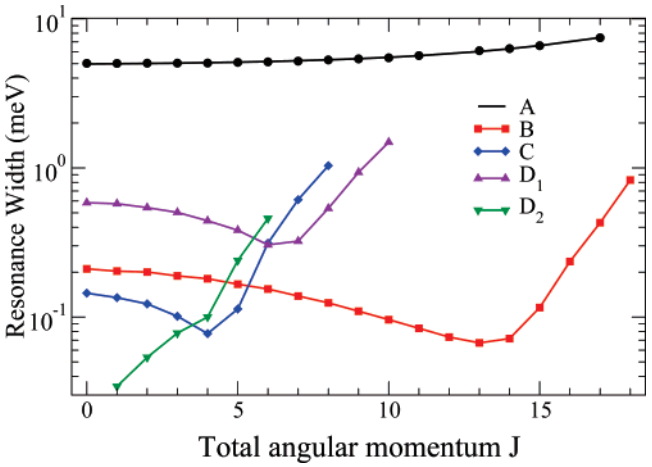

Figure 5. Resonance widths versus total angular momentum. The symbols have the same meaning as in Figure 4.

state from ref 3, we obtain $B_A = 0.181$ meV for the resonance A. For the resonances B, C, and D, the diatomic distance r can be fixed equal to that of the exit channel van der Waals minimum[56] very close to the HF equilibrium distance. The expectation values of R can be obtained using one-dimensional resonance wave functions calculated by the adiabatic model in section III.B (5.7, 7.3, and 6.7 a_0 for B, C, and D, respectively) which gives $B_r = 0.120$, 0.074, and 0.088 meV. These values are in agreement with the "exact" scattering data of Table 1 to within a few percent which confirms the reliability of the adiabatic model. The difference for the resonance A is somewhat larger (~10%) because of the approximation of constant R which is less reliable near the transition state geometry.

Figure 5 shows the resonance widths Γ_r as functions of J. The ratio

$$\Delta J \approx \frac{\Gamma_r(J)}{B_r(2J+1)} \tag{9}$$

is a semiclassical estimate for the number of partial waves affected by the resonance in the vicinity of the resonance energy.[57] It can be used as a criterion to classify resonances based on their effects on reactive observables. If ΔJ is large (broad resonance), the resonance affects many partial waves and a single broad feature appears as a result of a convolution of several overlapping resonances of different J. When ΔJ is less than one (narrow resonance), the resonance contribution comes from a single partial wave and the resulting peaks are isolated and correspond to well-defined values of J.[57] It has been recently demonstrated[58] that, if the value of the ratio (9) is close to one,[59,60] the ICS exhibits a broad sinusoidal behavior, termed Regge oscillations.[61] The maxima of the Regge oscillations do not always coincide with the resonance energies. Using the data of Figure 5 and the rotational constants of Table 1, we classify the resonances B, C, and D as narrow for almost all J. The resonance A is of an intermediate type: it is broad at $J \leq 5$, whereas at higher J, the ratio (9) approaches one. Therefore, we expect Regge oscillations of the ICS at the energies of the resonance A at $J > 5$.

Figure 5 shows that the lifetimes of all resonances (excluding A) exhibit distinct maxima as functions of J. This indicates two competing decay mechanisms (see also ref 62). At moderate J, the resonances are below the HF($v' = 3$) threshold (marked by the dashed line in Figure 4), and they decay by vibrational predissociation loosing one quantum of HF vibration and populating the HF($v' = 2, j'$) levels.[23] The vibrational predissociation is a slow process with the rate determined by the overlap of the resonance wave function with the rovibrational states of the HF product[51] rather than by the energy gaps between the states. As a result, the resonances shown in Figure 5 are narrow, and their widths do not change much with J. The resonances above the threshold may decay via tunneling through the centrifugal barrier (the so-called shape mechanism). The height of the barrier increases with J as $J(J+1)/2m_{HF-D}R_b^2$, where R_b is the value of the atom−molecule separation at the barrier. On the other hand, the resonance energy increases as $J(J+1)/2m_{HF-D}R_r^2$, where R_r is the expectation value of R averaged over the 1D resonance wave function trapped before the barrier. Since $R_b > R_r$, the effective barrier height decreases and the tunneling rate increases with J.[32] The tunneling mechanism is more efficient than the vibrational predissociation at the energies above the threshold. It is responsible for the fast increase of the resonance widths at large J values (see Figure 5). Finally, we note that the resonance D can also decay via a mechanism involving the inelastic transition ($v' = 3, j' = 1$) → ($v' = 3, j' = 0$) which releases ~4.8 meV of energy, enough to break the weak HF($v' = 3$)···D van der Waals bond. This is rotational predissociation[53,63,64] driven by the anisotropy of the HF···D interaction potential.

The width of the resonance A, on the contrary, increases with J monotonically suggesting a different decay mechanism. In ref 3, it was found that this state decays mainly by tunneling through the barrier along the F−H_2 angular coordinate, and the dependence $\Gamma_r(J)$ was fitted by an exponential function $\Gamma_r(J) = a + b(\exp(cJ) - 1)$. Fitting the results of Figure 5, we obtain the values 4.97, 0.79 meV, and 0.205 for the parameters a, b, and c, respectively. The comparison with the results of ref 9 obtained with the SW PES shows that our parameter c is smaller by a factor of ~4. The convolution of several J-shifted A resonances calculated on PESIII produces a shoulder-like feature[65] in the dependence of the ICS on the collision energy, in contrast with the broad peak observed in the calculation with the SW PES.[3,10] This follows from the fact that the resonance widths calculated on PESIII change less significantly with J.[65]

The decay probabilities (7) determine to what extent a resonance participates in the reaction and is therefore an important parameter to asses the relevance of resonance effects on the reaction dynamics. Figure 6 shows the decay probabilities

Figure 6

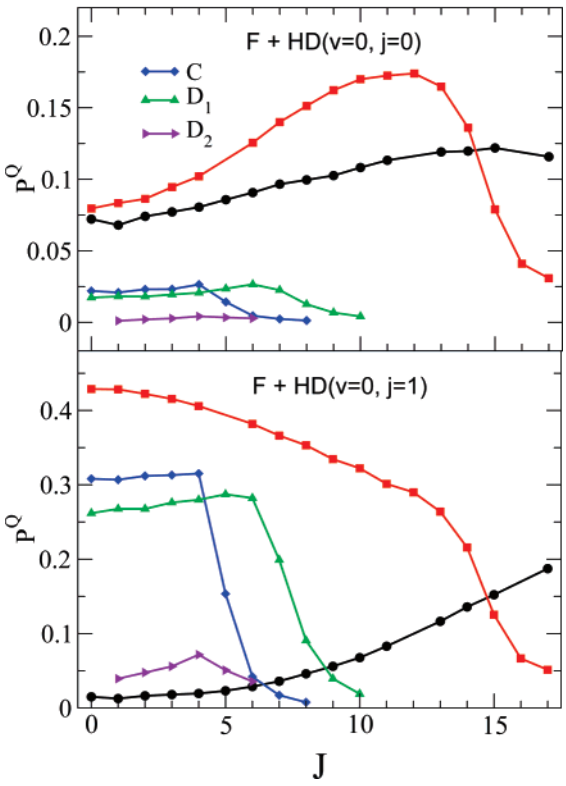

Figure 6. Angular momentum dependence of the decay probabilities (eq 7) summed over over all open channels of the HF product for the F + HD($v = 0, j = 0$) (upper panel) and F + HD($v = 0, j = 1$) (lower panel) reactions. The symbols label different metastable states as in Figures 4 and 5.

as functions of J for the reaction of F with HD($v = 0$) in the ground (upper panel) and in the first excited (lower panel) rotational states. Higher rotational states of HD ($j \geq 2$) are not populated in molecular beam experiments on the F + HD reaction and are not analyzed in this work. Figure 6 shows that decay probabilities of the resonances C and D become very small for $J > 8$. The decrease correlates with the increase of their widths up to 1−2 meV (see Figure 5). This suggests that the effects of the resonances C and D on reactive cross sections are weak at higher J. However, they may be important at low J, especially for the reaction F + HD ($v = 0, j = 1$) when the resonances C and D decay significantly into the entrance channel.

On the other hand, the decay probabilities of the resonances A and B are non-negligible even at large J. This suggests that they may influence reaction cross sections in a wide range of collision energies. The resonances A and B are present in the reaction of F with both HD($v = 0, j = 0$) and HD($v = 0, j = 1$), although their behavior with J is different. The decay probability of the resonance B in the reaction F + HD($v = 0, j = 1$) is large at small J and smoothly goes to zero as J increases, whereas that in the reaction F + HD($v = 0, j = 0$) shows a flat maximum at $J \sim 10$. Otherwise, the decay probability of the A peak in the reaction F + HD($v = 0, j = 1$) is near zero at low J but it increases exponentially for $J > 10$. At the same time, the decay probability of the same resonance in the reaction F + HD($v = 0, j = 0$) does not change with J. As will be shown in section IV.B, this behavior is responsible for different reactivity of the two rotational states of HD. As soon as the $v' = 3, j' = 0$ state of HF becomes energetically available, all resonances start to decay into this channel, except for the resonance A which decays into the $v' = 2$ channel. The impact of this behavior on the reactive scattering cross sections will be discussed in section IV.B.

In summary, we have shown that the narrow resonances C and D can only affect reaction probabilities at low J and therefore will give small effects in the reactive observables only in a limited range of energies, especially for the reaction of HD($v = 0, j = 0$). A similar tendency was also observed in the F + H_2 reaction.[33] In that work, we showed that the decay probabilities of the resonances correlating with higher rotational states of the HF product approach zero at lower J. For this reason, we restrict the Q-matrix analysis to the lowest exit-channel resonances B, C, and D. On the contrary, the resonances A and B affect many partial waves and collision energies well above the barrier height. Resonance effects in the F + HD($v = 0, j = 0$) reaction are expected to be stronger at low collision energies because of the higher decay probabilities.

IV. Discussion

A. Isotope Effects in Resonance Dynamics. It is interesting to compare the $J = 0$ resonance parameters discussed in section III.A with the corresponding resonances found in ref 33 (and reproduced in Table 1) for the F + H_2 reaction on the same PES. This will allow us to understand the effects of the isotopic substitution on the dynamics of reactive scattering resonances using simple kinematic arguments.

Because of the isotopic substitution, the zero-point energy E^0 of the reactants becomes lower. Using a harmonic approximation, we obtain

$$\Delta E^0 = \bar{E}^0_{H_2} - E^0_{HD} \approx \left[1 - \left(\frac{m_H + m_D}{2m_D}\right)^{1/2}\right]\bar{E}^0_{H_2} \simeq 35.9 \text{ meV} \quad (10)$$

where $\bar{E}^0_{H_2}$ is the zero-point energy of the H_2 molecule. The result of eq 10 is in agreement with the "exact" value of 35.6 meV from dynamical calculations. To estimate the isotopic shift of the resonance A, ΔE^0_A, we use the harmonic approximation for vibrational modes of the triatomic FHD complex. Replacing the ratio of the two-body reduced masses of eq 10 with the ratio of the hyperspherical three-body reduced masses of FHH and FHD (μ_{FHH}/μ_{FHD}), we obtain

$$\Delta E^0_A = \bar{E}^0_A - E^0_A \approx \left[1 - \left(\frac{m_H(m_F + m_H + m_D)}{m_D(m_F + 2m_H)}\right)^{1/4}\right]\bar{E}^0_A \quad (11)$$

where $\bar{E}^0_A$ and E^0_A are the zero point energies of the FH_2 and FHD triatomic complexes (see Figure 7), respectively. Using the data of Table 1 and the energy of the classical collinear saddle point[3] (see section III.C), we obtain the energy $\bar{E}^0_A \simeq$ 199.0 meV and $\Delta E^0_A \simeq$ 29.7 meV. The isotopic substitution therefore shifts the resonance A toward higher translational energies by ~5.9 meV, in good agreement with the "exact" value of 6.4 meV from Table 1. The energies of the exit channel resonances B, C, and D do not change much because the isotopic substitution HF···H → HF···D does not affect the dominant HF stretching mode. Equation 10 shows that the ground state of the reactants is shifted down by ~35.6 meV. This value is a fairly good estimate of the isotopic shift from Table 1.

The remaining discrepancies are likely due to the bound levels of HF···H(D) in shallow exit-channel van der Waals wells. The eigenvalues of the 2D Hamiltonian (adiabatic curves) in Figure 2 are almost identical for HF···D and HF···H (except for a small

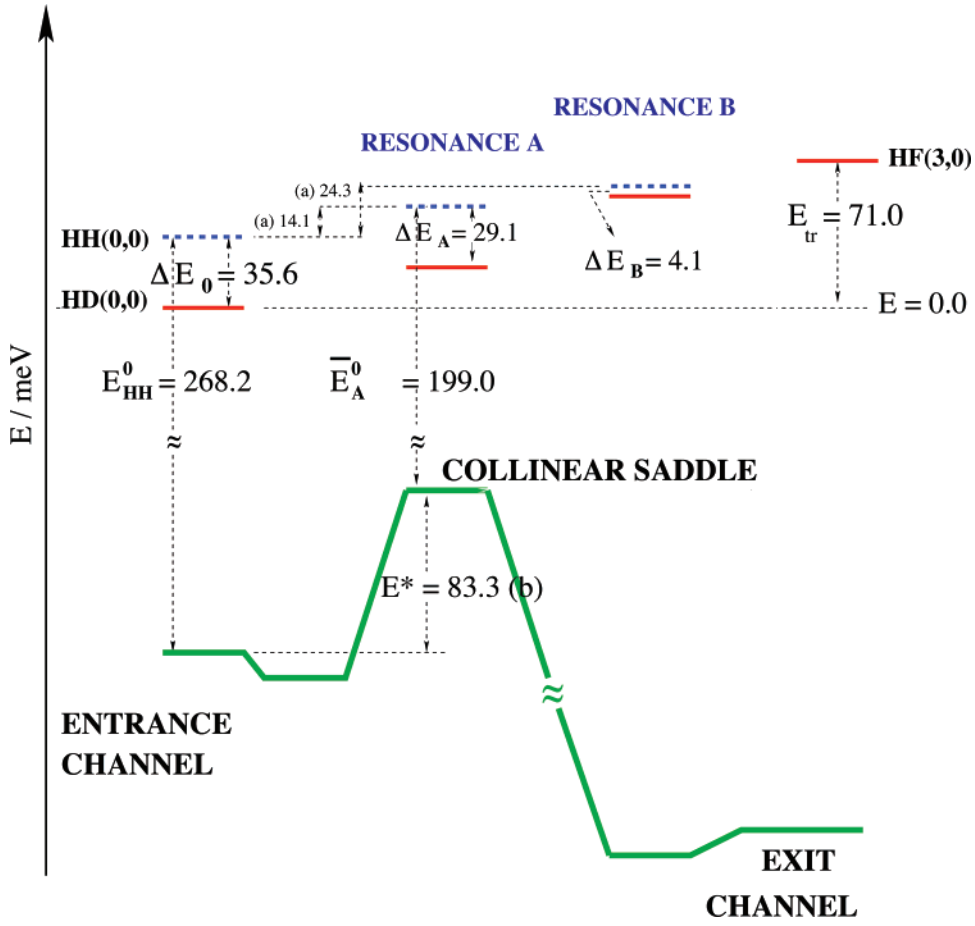

Figure 7. The energy diagram of the F + HD reaction from PESIII. The energy levels of the F + H_2 reaction are also shown by dashed lines. The energies labeled (a) were taken from ref 33 and those labeled with (b) were taken from ref 3.

difference of the reduced mass entering the centrifugal term in eq 6, which is small at low l). At $J = 0$, the resonances B and C are characterized by $l = 0$ (the resonance D correlates to $l = 1$). Therefore, we can assume that isotopic substitution does not affect the potential curves shown in Figure 2. All the difference between the energies of HF···D and HF···H thus comes from the stretching motion of the heavier D atom relative to the HF fragment. Therefore, we can apply the harmonic approximation once again to this particular local mode. The mass ratio is now that of the atom−diatom two-body reduced masses in the exit channel arrangment: m_{HF-H}/m_{HF-D}. The required zero-point energies of the HF−H stretching modes $\bar{E}^0_{B,C,D}$ can be directly evaluated as the difference between the energy levels in parentheses (Table 1) and the minima of the corresponding adiabatic wells in Figure 2. They are 12.5, 22.9, and 8.7 meV for B, C, and D, respectively. The isotopic shift

$$\Delta E^0_{B,C,D} \approx \left[1 - \left(\frac{m_H(m_F + m_H + m_D)}{m_D(m_F + 2m_H)}\right)^{1/2}\right] \bar{E}^0_{B,C,D} \quad (12)$$

is equal to 3.4, 6.3, and 2.4 meV for the resonances B, C, and D, respectively. Taking into account the downward shift of the H_2 zero-point energy discussed above, we observe that the resonances B, C, and D are shifted to higher collision energies by 32.2, 29.3, and 33.2 meV, respectively. The comparison with the data of Table 1 shows that this estimate is accurate for the B resonance (31.5 meV) but less so for the resonances C and D (34.8 and 31.9 meV, respectively). This might be due to the strong coupling between the adiabatic states[32] and the breakdown of the adiabatic picture. The strongly mixed nature of these states is also evident from the wave function plots in Figure 3 (see section III.B).

In summary, the isotopic substitution shifts resonances in the exit channel to higher energy by ~35 meV. The energy of the resonance A is affected to a lesser extent. As a consequence, the resonances A and B become degenerate at higher collision energies (and partial waves J) than for the F + H_2 reaction where resonance B is weakly coupled to the entrance channel. In addition, at the value of $J = 18-19$ when the resonances A and B cross, they decay into different vibrational manifolds ($v' = 2$ and 3, respectively). This indicates that their interaction is much weaker than in the F + H_2 reaction.[43] Because of the larger reduced mass and the reduced tunneling rate of the D atom, the isotopic substitution increases the resonance lifetime. The exit-channel resonances B, C, and D are thus expected to survive up to higher J and contribute significantly to the dynamics of the F + HD reaction.

Finally, we point out that the van der Waals well in the exit channel does not produce any DF···H quasibound states relevant for the reactivity of the F + HD system. The DF + H channel is more exoergic than the HF + D channel, so that the DF($v' = 3$, j') manifold is at a lower energy than the reactants. The metastable states supported by the adiabatic curves of DF($v' = 4$, j') are very weakly coupled to the entrance channel, because of the large difference in vibrational quantum numbers and unfavorable Frank-Condon factors. As a result, the resonances in the DF−H channel affect only nonreactive collisions of DF molecules with H atoms.

B. Resonance Effects on the Reactive Observables. One aspect that makes the F + HD reaction unique is a large number

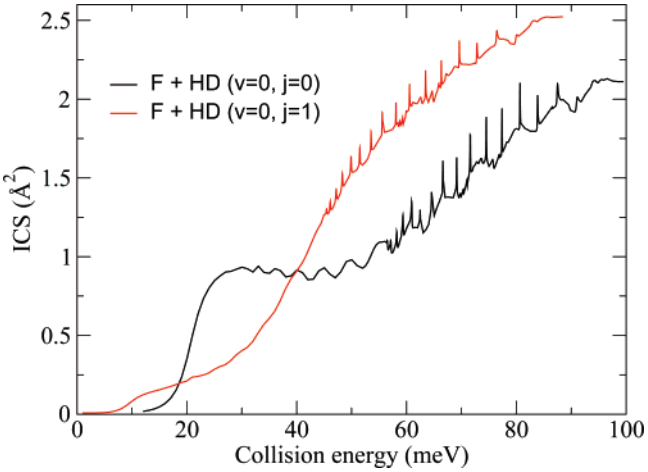

Figure 8. Integral cross sections for the F + HD($v = 0$, $j = 0$) (dark line) and the F + HD($v = 0$, $j = 1$) (red line) reactions summed over all the open channels of the HF product as functions of the collision energy.

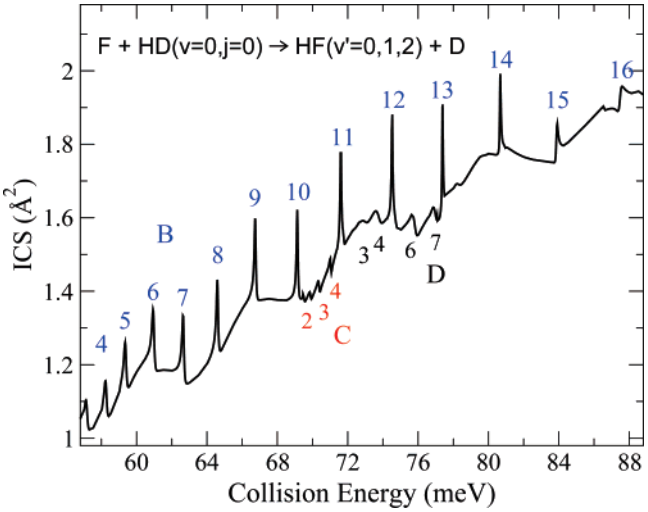

Figure 9. Integral cross sections for the F + HD($v = 0$, $j = 0$) reaction summed over all open channels of HF($v' = 0,1$ and 2) in the region of collision energies where the exit-channel resonances occur. The numbers denote the value of the total angular momentum of the resonance.

of experimental results available including state-resolved angular distributions, integral cross sections, and thermally averaged rate constants. In this section, we will focus on the influence of resonances on reactive observables. We calculated ICSs on the energy grid of 0.5 meV which is dense enough to resolve the broad resonance A but not the narrower long-lived resonances of the exit channel. We note that because of their small widths (see Table 1) such resonances influence only a single resonant partial wave contribution (J_r) to the ICS, and the approximation of isolated narrow resonance is accurate. Therefore, in the vicinity of a narrow resonance, we only need to evaluate the cross section at $J = J_r$, whereas a simple linear interpolation can be used to compute other (nonresonant) partial waves. With this procedure, we were able to obtain total ICS with the energy resolution of 0.02 meV. Numerical tests show that the errors introduced by the linear interpolation are ~1%.

Figure 8 shows the ICS for the reaction F with HD in the ground and the first excited rotational levels summed over all open product states. For the reaction F + HD ($v = 0$, $j = 0$) below 30 meV, the width of the resonance A is nearly independent of J and large enough to form a step-like convolution feature,[65] which is also observed in the experiment.[10] At higher energies, higher partial waves contribute and the ratio (9) decreases. Regular sinusoidal oscillations appear when the critical value of $\Delta J = 1$ is reached at ~30 meV. These structures are known as Regge oscillations[61] and they have recently been analyzed in the F + H_2 reaction[58] in a narrower range of collision energies.

At collision energies above 55 meV, the ICS shows a progression of narrow resonances superimposed on Regge oscillations. For the reaction of F with HD($v = 0$, $j = 1$), the resonance A is only barely visible while the pattern of long-lived resonances B−D is more pronounced than in the reaction of HD($v = 0$, $j = 0$) and they are shifted at lower collision energy (≈11 meV).

Figure 9 shows more details of long-lived resonances in the F + HD($v = 0$, $j = 0$) reaction. In this figure, we plot the ICS summed over all open vibrational states of HF except $v' = 3$ that will be analyzed separately. Each major peak is due to the resonance B corresponding to a specific value of J. The weak oscillations between 70 and 80 meV are due to low partial waves of the resonances C and D. These features are reminiscent of the $J = 0$ Fano profiles shown in Figure 1, but their intensity is much smaller due to the partial wave averaging. The resonance density is high in this collision energy range and many resonance patterns overlap which is the reason why not all of the peaks shown in Figure 9 can be assigned a quantum number.

We note that the resonance enhancement of the ICS presented in Figures 8 and 9 is at most 15% of the total reaction cross section. It may therefore be difficult to observe the resonances experimentally. On the other hand, the signature of the resonances is typically more pronounced in state and angle-resolved cross sections.[57] In particular, the experimental studies[4,19,21] revealed large oscillations in state-resolved cross sections for the formation of HF($v' = 3$) products near threshold. This contradicts the theoretical calculations[10,13] which predict that the HF($v' = 3$) channel accounts for less than 10% of the total reactivity.

Figure 10 shows the ICS for the formation of HF($v' = 3$) in the reaction of HD in both the ground and the first excited rotational states. At the HF($v' = 3$) threshold, the background reactivity of HD($v = 0$, $j = 0$) is very low (around 0.01 Å^2), and only weak structures due to the resonances C and D are present in the ICS. However, the situation changes when the resonance B crosses the HF($v' = 3$, $j' = 0$) threshold at $J = 14$ and begins to decay preferentially into this channel. As a result, the corresponding resonance peak in Figure 10 makes the ICS increase by a factor of 3. For the reaction of rotationally excited HD, the long-lived resonances C, D_1, and D_2 have a stronger impact on the ICS, as shown in the inset of the lower panel of Figure 10.

As mentioned earlier, sharp forward−backward features observed in the energy dependence of the DCS[2,19] between 1 and 2 kcal/mol, might be a signature of long-lived resonances. Figure 11 shows 3D plots of vibrationally resolved DCS for the production of HF($v' = 2$ and 3) in the reaction of F with HD($v = 0$, $j = 0$) as functions of the angle and energy. The collision energy interval is centered around the resonance B at $J = 14$ with an energy resolution of 0.02 meV. In order to reproduce accurately the interference between different partial waves, a larger number of Ω projections ($\Omega_{max} = 5$ see section II) and total angular momenta (26) was included in the calculations.

The DCS for $v' = 2$ (Figure 11, upper panel) changes rapidly near the resonance energy, although not in a way that shows distinct forward−backward features. On the other hand, the DCS

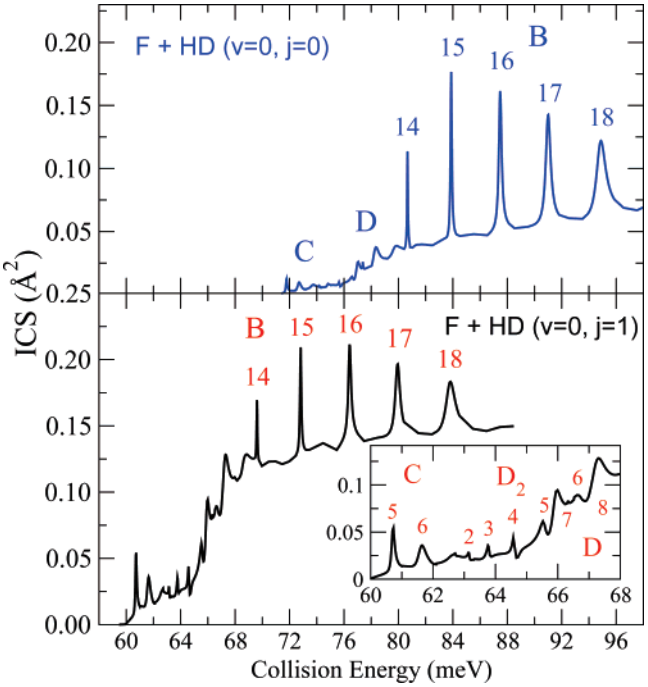

Figure 10. Integral cross sections for the F + HD($v = 0, j = 0$) (upper panel) and for the F + HD($v = 0, j = 1$) (lower panel) reactions summed over all open channels of the HF($v' = 3$) product. The numbers have the same meaning as in Figure 9. The inset in the lower panel shows the reactive ICS near threshold.

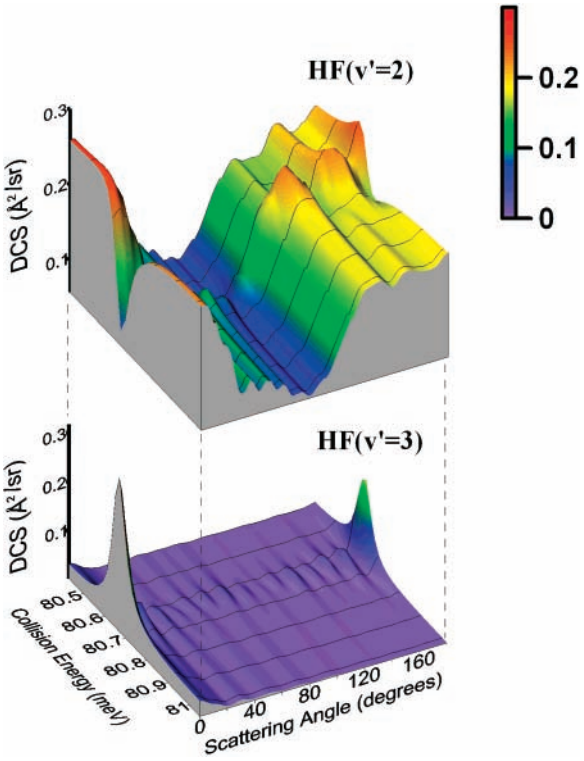

Figure 11. Differential cross sections for the F + HD($v = 0, j = 0$) reaction summed over all open channels of HF($v' = 2$) (upper surface) and HF($v' = 3$) (lower surface) as functions of the scattering angle and the collision energy. The collision energy corresponds to the resonance B at $J = 14$ in the neighborhood of the HF($v' = 3, j' = 0$) threshold.

for the production of HF($v' = 3$) is clearly forward−backward peaked. We found that the DCS depends on the scattering angle θ at the resonance energy E_r as

$$\sigma(\theta, E_r) \propto |P_{J_r}(\cos\theta)|^2 \quad (13)$$

where $P_{J_r}(\cos\theta)$ is the Legendre polynomial of J_rth order. The dependence (13) is characteristic of differential scattering near a narrow resonance.[23] We conclude that the behavior of the DCS in the $v' = 2$ and $3'$ channels is dramatically different. The former is dominated by the resonance A, which leads to a complicated interference pattern,[2,3] whereas the latter is strongly influenced by the near-threshold narrow resonances in the exit channel.

V. Conclusions

In summary, we have performed a study of resonances in the F + HD reaction. Using the lifetime matrix formalism, we have calculated the positions and lifetimes of the most important reactive scattering resonances in the total collision energy range of 10−100 meV. The quasibound states observed are assigned using the adiabatic model (Figure 2) as well as variational and stabilization calculations of the bound states and wave functions (Figure 3) of the HF($v = 3$)···D van der Waals complex. The behavior of resonances at nonzero total angular momentum J (Figures 4 and 5) is analyzed systematically. Simple kinematic arguments are used to model the effect of isotopic substitution on the resonances. It is shown that near-threshold Feshbach resonances B, C, and D can decay via tunneling through centrifugal barriers or by rotational predissociation. The latter mechanism is present for the resonances D correlating to the excited rotational levels of HF.

We found that, while the lifetime and partial width of the resonance A do not change much with J, the exit-channel resonances C and D become decoupled from the entrance channel already at small J (see Figure 6). As a result, the quasibound states C and D affect the reactive ICS in a limited range of collision energies of about 10 meV near the HF($v' = 3$) threshold. These results are in agreement with our previous findings for the F + H_2 reaction.[33] Unlike for F + H_2, the resonance B in the F + HD system survives up to much higher $J \sim 20$ and its influence can be clearly observed over the whole energy region studied in this work (see Figure 8).

The HF($v' = 2$) products are mainly affected by the transition state resonance A which decays almost exclusively into that channel, with a minor contribution from the resonance B. We demonstrated that the ICS for the reaction to form HF($v' = 3$) products near threshold (Figure 10) is dominated by decay of the exit-channel resonances B, C, and D. The reactive angular distributions for this vibrational state are forward−backward peaked (Figure 11) due to the formation of long-lived metastable complexes. This explains qualitatively the experimental observations.[2,18,19] On the contrary, the angular distributions of HF($v' = 2$) are not significantly affected by the exit-channel resonances.

The transition state resonance A is relevant only for the reaction of the ground rotational state of HD. It produces a broad step-like feature in the ICS at low energies and Regge oscillations at higher energies (see Figure 8). On the contrary, the long-lived resonances are important for the reaction of both the ground and rotational excited states of the reactants, so that the resonance features can also be observed in reactive cross sections from the HD($v = 0, j = 1$) state. This is particularly true of the resonances C and D (Figure 10). Although the resonance contribution to the total ICS is small (∼10%), it becomes more significant for state-resolved cross sections in the HF($v' = 3$) channel which are resonantly enhanced by a factor of 3.

Theoretical simulations of reactive ICSs in the energy range investigated should take into account the energy spread of the beam which is of the order of several meV.[17−21] As a result of this averaging over collision energy, narrow peaks seen in Figure 10 will be smeared and transformed into broad structures. We note that resonance partial widths (and in particular the decay probabilities) are very sensitive to fine details of the PES. For example, some of the recently published PESs[15] have an exit channel vdW well that is too shallow to support some of the metastable states studied in this work. It is therefore possible that small changes of the PES in the exit channel region can dramatically affect the long-lived resonances and their impact on reactivity. In spite of the high resonance density at the HF($v' = 3, j' = 0$) threshold energy (see Figure 10), a translational averaging of the data presented in this work is unlikely to reproduce the high HF($v' = 3$) yield observed in the experiments.[18,19] We have demonstrated in section IV.B that this is due to the small decay probability of the resonances into the entrance channel. However, our calculations do provide an insight into the role of narrow resonances in the near-threshold reaction dynamics of the F + HD reaction.

One flaw of the SW PES (and therefore of PESIII[12]) is that it inadequately describes the experimental exothermicity[15] which makes the comparison with experimental data difficult. As a result, all resonance patterns in the exit channel are artificially shifted by ∼11 meV. The shift will move the energy of the crossing between the resonance A and B (see Figure 4) down to $J \approx 15$ (instead of 18, as reported in this work). At $J = 15$, the resonance B still decays significantly into the HF($v' = 2$) channel, like the resonance A. Therefore, on a more accurate PES, the resonances A and B may interact and give rise to a strong forward enhancement of the DCS[66] due to the constructive interference of the two resonances. This, in turn, may result in strong forward peaks in the HF($v' = 2$) DCS around 70 meV that were observed experimentally.[2,19,18]

Although it was estimated[18,19] that HD($v = 0, j = 1$) accounts for less than 20% of the experimental beam, this state may be relevant in numerical simulations because of its higher reactivity to form HF($v' = 3$) products. The internal energy of HD in the first excited rotational state is higher, and the resonances A−D discussed in this work will occur at lower collision energies.[67] In addition to the exothermicity shift cited above, the energy range where forward−backward peaks appears in the experiment coincides with the energy range of the long-lived resonances studied in this work. This suggests that these Feshbach resonances may play a crucial role in the explanation of the experimental results of refs 2, 18, and 19.

In a recent study,[68] a new ab initio F−H_2 PES[69] with the correct exothermicity and a modified exit channel has been constructed. The probabilities for the F + H_2 reaction at $J = 0$ obtained with the new PES confirm the relevance of the exit-channel resonances studied in our previous work[33] but predict a much higher yield of the HF($v' = 3$) products. Our results lead us to conclude that the F + HD system is another excellent candidate to look for the signatures of Feshbach resonances, and it is our hope that this work will stimulate further theoretical and experimental studies of the F + HD reaction. Finally, we hope that the analysis of F + HD resonances made in this work can be useful to understand the dynamics of other heavier chemical systems (e.g., O + HCl and Li + HF)[70,71] where deeper vdW wells may have even stronger influence on the reactions.

Acknowledgment. The authors thank Dr. A. Simoni (Rennes) for providing his code for bound state calculations, Prof. A. Aguilar (Barcelona), and Prof. R. V. Krems (Vancouver, BC) for helpful comments on the manuscript. This work was supported by Italian ASI and MUR through PRIN and FIRB grants and Russian Basic Research Fund (Grant No. 05-03-32173). Support from the Killam postdoctoral fellowship to T.V.T. and from Russian Science Support Foundation to A.A.B. is gratefully acknowledged. The calculations of resonance lifetimes were allocated at Western Canada Research Grid (WESTGRID).

References and Notes

(1) Neumark, D. M.; Wodtke, A. M.; Robinson, G. N.; Hayden, C. C.; Shobatake, K.; Sparks, R. K.; Schafer, T. P.; Lee, Y. T. *J. Chem. Phys.* **1985**, *82*, 3067.
(2) Skodje, R. T.; Skouteris, D.; Manolopoulos, D. E.; Lee, S.-H.; Dong, F.; Liu, K. *Phys. Rev. Lett.* **2000**, *85*, 1206.
(3) Skodje, R. T.; Skouteris, D.; Manolopoulos, D. E.; Lee, S.-H.; Dong, F.; Dong, K. *J. Chem. Phys.* **2000**, *112*, 4536.
(4) Dong, F.; Lee, S.-H.; Liu, K. *J. Chem. Phys.* **2000**, *113*, 3633.
(5) Manolopoulos, D. E.; Stark, K.; Werner, H. J.; Arnold, D. W.; Bradforth, S. E.; Newmark, D. M. *Science* **1993**, *262*, 1852.
(6) Takayanagi, T.; Wada, A. *Chem. Phys. Lett.* **2001**, *348*, 514.
(7) Stark, K.; Werner, H. J. *J. Chem. Phys.* **1996**, *104*, 6515.
(8) Chao, S. D.; Skodje, R. T. *Theor. Chem. Acc.* **2002**, *108*, 273.
(9) Liu, K.; Skodje, R. T.; Manolopoulos, D. E. *Phys. Chem. Comm.* **2002**, *5*, 27.
(10) De Fazio, D.; Aquilanti, V.; Cavalli, S.; Aguilar, A.; Lucas, J. M. *J. Chem. Phys.* **2006**, *125*, 133109.
(11) Aquilanti, V.; Cavalli, S.; Pirani, F.; Volpi, A.; Cappelletti, D. *J. Phys. Chem.* **2001**, *105*, 2401.
(12) Aquilanti, V.; Cavalli, S.; De Fazio, D.; Volpi, A.; Aguilar A.; Lucas, J. M. *Chem. Phys.* **2005**, *308*, 237.
(13) Tzeng, Y. R.; Alexander, M. H. *J. Chem. Phys.* **2004**, *121*, 5183; *Phys. Chem. Chem. Phys.* **2004**, *6*, 5018.
(14) Xie, T.-X.; Zhang Y.; Han, K.-L. *Chem. Phys. Lett.* **2004**, *398*, 313.
(15) Hayes, M.; Gustafsson, M.; Mebel, A. M.; Skodje, R. T. *Chem. Phys.* **2005**, *308*, 259.
(16) Takayanagi, T.; Kurosaki, Y. *Phys. Chem. Chem. Phys.* **1999**, *1*, 1099.
(17) Lee, S.-H.; Dong, F.; Liu, K. *J. Chem. Phys.* **2002**, *116*, 7839.
(18) Lee, S.-H.; Dong, F.; Liu, K. *J. Chem. Phys.* **2006**, *125*, 133106.
(19) Lee, S.-H.; Dong, F.; Liu, K. *Faraday Discuss.* **2004**, *127*, 49.
(20) Lee, S.-H.; Dong, F.; Liu, K. *J. Chem. Phys.* **2006**, *124*, 224312.
(21) Harper, W. W.; Nizkorodov, S. A.; Nesbitt, D. J. *J. Chem. Phys.* **2002**, *116*, 5622.
(22) Honvault, P.; Launay, J.-M. *J. Chem. Phys.* **2001**, *114*, 1057; **1999**, *111*, 6665.
(23) Castillo, J. F.; Manolopoulos, D. E. *Faraday Discuss.* **1998**, *110*, 119.
(24) Takayanagi, T.; Kurosaki, Y. *J. Chem. Phys.* **1998**, *109*, 8929; *Chem. Phys. Lett.* **1998**, *286*, 35.
(25) Takayanagi, T.; Wada, A. *Chem. Phys. Lett.* **2001**, *338*, 195.
(26) Dobbyn, A. J.; McCabe, P. J.; Connor, N. L.; Castillo, J. F. *Phys. Chem. Chem. Phys.* **1999**, *1*, 1115.
(27) Sokolovsky, D. *Phys. Rev. A* **2000**, *62*, 024072.
(28) Takayanagi, T. *Chem. Phys. Lett.* **2006**, *433*, 15.
(29) Wigner, E. P. *Phys. Rev.* **1955**, *98*, 145.
(30) Smith, F. T. *Phys. Rev.* **1960**, *118*, 349.
(31) Chao, S. D.; Skodje, R. T. *J. Chem. Phys.* **2003**, *119*, 1462.
(32) Aquilanti, V.; Cavalli, S.; Simoni, A.; Aguilar, A.; Lucas, J. M.; De Fazio, D. *J. Chem. Phys.* **2004**, *121*, 11675.
(33) Aquilanti, V.; Cavalli, S.; De Fazio, D.; Simoni, A.; Tscherbul, T. V. *J. Chem. Phys.* **2005**, *123*, 054314.
(34) Aquilanti, V.; Candori, R.; Cappelletti, D.; Luzzatti, E.; Pirani, F. *Chem. Phys.* **1990**, *145*, 293.
(35) Aquilanti, V.; Cavalli, S.; De Fazio, D.; Volpi, A.; Aguilar, A.; Giménez, X.; Lucas, J. M. *Phys. Chem. Chem. Phys.* **2002**, *4*, 401; *Chem. Phys. Lett.* **2003**, *371*, 504.
(36) Alexander, M. H.; Manolopoulos, D. E.; Werner, H.-J. *J. Chem. Phys.* **2000**, *113*, 11084.
(37) Hartke, B.; Werner, H.-J. *Chem. Phys. Lett.* **1997**, *280*, 430.
(38) The entrance channel of the PESs used in refs 36 and 37 is about 16 meV lower than that of PESIII.[12] Thus many of the resonances described in this work will be shifted to higher collision energies in calculations with the PESs of refs 36 and 37.
(39) Aquilanti, V.; Cavalli, S.; De Fazio, D. *J. Chem. Phys.* **1998**, *109*, 3792.
(40) De Fazio, D.; Aquilanti, V.; Cavalli, S. *Int. J. Quantum Chem.* **2003**, *93*, 91.

(41) Aquilanti, V.; Cavalli, S. De Fazio, D.; Volpi, A.; Aguilar, A. Giménez, X.; Lucas, J. M. *J. Chem. Phys.* **1998**, *109*, 3805; *Phys. Chem. Chem. Phys.* **1999**, *1*, 99.
(42) Aquilanti, V.; Cavalli, S.; De Fazio, D.; Volpi, A. *Adv. Quantum Chem.* **2001**, *39*, 103.
(43) Sokolovski, D.; Sen, S. K.; Aquilanti, V.; Cavalli, S.; De Fazio, D. *J. Chem. Phys.* **2007**, *126*, 084305.
(44) Cavalli, S.; De Fazio, D. *Phys. Scr.* **2007**, *76*, C21.
(45) Shimamura, I.; McCann, J. F.; Igarashi, A. *J. Phys. B* **2006**, *39*, 1847.
(46) Fano, U. *Phys. Rev.* **1961**, *124*, 1866.
(47) Balakrishnan, N.; Dalgarno, A. *J. Phys. Chem. A* **2003**, *107*, 7101.
(48) Bodo, E.; Gianturco, F. A.; Balakrishnan, N.; Dalgarno, A. *J. Phys. B* **2004**, *37*, 3641.
(49) Colbert, D. T.; Miller, W. H. *J. Chem. Phys.* **1992**, *96*, 1982.
(50) Castillo, J. F.; Manolopoulos, D. E.; Stark K.; Werner, H. J. *J. Chem. Phys.* **1996**, *104*, 6531.
(51) Delgado-Barrio, G.; Beswick, J. A. In *Structure and Dynamics of Non-Rigid Molecular Systems*; Smeyers, Y. G., Ed.; Kluwer: Dordrecht, The Netherlands, 1994; p 203.
(52) Reid, B. P.; Janda, K. C.; Halberstadt, N. *J. Phys. Chem.* **1992**, *92*, 587.
(53) Ashton, C. J.; Child, M. S.; Hutson, J. M. *J. Chem. Phys.* **1983**, *78*, 4025.
(54) Wilson, R. L.; Loh, Z. M.; Wild, D. A.; Bieske, E. J.; Buchachenko, A. A. *J. Chem. Phys.* **2004**, *121*, 2085.
(55) Grinev, T. A.; Buchachenko, A. A.; Kłos, J.; Bieske, E. J. *J. Chem. Phys.* **2006**, *125*, 114313.
(56) Manolopoulos, D. E. *J. Chem. Soc. Faraday Trans.* **1997**, *93*, 673.
(57) Miller, W. H.; Zhang, J. *J. Phys. Chem.* **1991**, *95*, 12.
(58) Sokolovski, D.; De Fazio, D.; Cavalli, S.; Aquilanti, V. *J. Chem. Phys.* **2007**, *126*, 121101.
(59) Note that the mathematical condition for Regge oscillations in ref 58 is given in the framework of the Regge pole formalism. The quantities defined in this work are related to those of ref 58 as $\mathrm{Im}\lambda \simeq \Delta J/2$.[60]
(60) Sokolovski, D.; Castillo, J. F. *Phys. Chem. Chem. Phys.* **2000**, *2*, 507.
(61) Macek, J. H.; Krstić, P. S.; Ovchinnikov, S. Y. *Phys. Rev. Lett.* **2004**, *93*, 183203.
(62) Sokolovski, D.; Msezane, A. Z. *Phys. Rev. A* **2004**, *70*, 032710.
(63) Jang, H. W.; Choi, S. E.; Light, J. C. *J. Chem. Phys.* **1994**, *100*, 4188.
(64) Choi, S.; Lester, M. I.; Jang, H. W.; Light, J. C. *J. Chem. Phys.* **1995**, *102*, 1981.
(65) Schatz, G. C. Sokolovski D.; Connor, J. N. L. *J. Chem. Phys.* **1991**, *94*, 4311.
(66) Sokolovski, D.; De Fazio, D.; Cavalli, S.; Aquilanti, V. *Phys. Chem. Chem. Phys.* **2007**, *9*, 5664.
(67) Ren, Z.; Che, L.; Qiu, M.; Wang, X.; Dai, D.; Harich, S. A.; Wang, X.; Yang, X.; Xu, C.; Xie, D.; Sun, Z.; Zhang, D. H. *J. Chem. Phys.* **2006**, *125*, 151102.
(68) Qiu, M.; Ren, Z.; Che, L.; Dai, D.; Harich, S. A.; Wang, X.; Yang, X.; Xu, C.; Xie, D.; Gustafsson, M.; Skodje, R. T.; Sun, Z.; Zhang, D. H. *Science* **2006**, *311*, 1440.
(69) Xu, C. X.; Xie, D. Q.; Zhang, D. H. *Chin. J. Chem. Phys.* **2006**, *19*, 96.
(70) Xie, T.; Wang, D.; Bowman, J. M.; Manolopoulos, D. *J. Chem. Phys.* **2002**, *116*, 7461.
(71) Parker, G. A.; Lagana, A.; Crocchianti, S.; Pack, R. T. *J. Chem. Phys.* **1995**, *102*, 1238.